ARCHIVE OF MECHANICAL ENGINEERING

DOI: 10.24425/ame.2026.157608 2026, Vol. 73, No. 1, pp. 149–166

Nam NGUYEN SY [1]

Dynamics of flexible overhead cranes: modeling and dynamic responses

Received 23 October 2025, **Revised** 7 January 2026, **Accepted** 23 January 2026, **Published online** 9 March 2026

Keywords: overhead crane, flexible, dynamic, vibration, beam

This study presents a nonlinear dynamic model of a flexible overhead crane operating in a vertical plane. The model simultaneously considers the flexural deformation of the main girder, the axial elongation of the hoisting cable, and the effects of internal damping. The equations of motion are formulated as a system of nonlinear ordinary differential equations (ODEs), allowing efficient simulation of the system's dynamic response, vibration behavior and stability characteristics. Numerical analyses are conducted for both undamped and damped cases. The results show that the elastic deformation of the cable is the primary source of beam vibration, while the payload sway also contributes to the overall oscillation. Including cable elasticity slightly increases the maximum beam deflection but significantly amplifies elastic oscillations. When damping is introduced, both cable and beam oscillations are reduced, and can be reduced to static deformation with increasing damping. The study provides a compact yet accurate modeling framework and offers useful insights for the integrated control of elastic and sway vibrations in flexible overhead cranes.

1. Introduction

Overhead cranes are among the most important electromechanical systems in industrial manufacturing, shipyards, and construction, used for lifting and transporting heavy loads within a limited workspace. During operation, the crane performs multiple coordinated motions–the bridge, trolley, and hoisting mechanisms–which interact dynamically. This configuration makes the system nonlinear and underactuated, leading to complex vibrations, including payload sway and elastic oscillations of the bridge girder and the hoisting cable [1–3]. Such vibrations reduce position-

✉ Nam NGUYEN SY, e-mail: namns@huce.edu.vn

[1] Hanoi University of Civil Engineering, Hanoi, Vietnam

ing accuracy and operational efficiency. They also shorten structural lifetime and compromise safety.

Traditionally, most crane models consider the system to be rigid, where the payload is modeled as a single or double pendulum suspended from a trolley, while both the girder and the cable are assumed inextensible. Based on this simplification, numerous studies have focused on anti-sway control using classical and modern approaches, such as PID, LQR, sliding-mode, model predictive control (MPC), and input shaping [4–8]. These methods are effective for light loads and stiff structures. However, for large-span cranes or those with slender, flexible girders, neglecting structural elasticity leads to noticeable discrepancies between predicted and actual behavior [9, 10].

Recent research has demonstrated that the flexibility of the main girder strongly influences the crane's dynamic response. In [11], the bridge girder was modeled as an Euler–Bernoulli beam subjected to a moving trolley with a suspended load, showing that both trolley speed and payload mass significantly affect the girder deflection and natural frequencies. Later studies [12, 13] adopted the Timoshenko beam theory, which accounts for shear deformation and rotary inertia, and showed improved accuracy for girders with moderate slenderness. These investigations revealed that crane vibrations are not limited to payload sway but include bending and shear modes, resulting in multi-frequency coupled oscillations during operation.

Another important source of vibration is the elastic deformation of the hoisting cable. Earlier works typically assumed the cable to be inextensible, but in reality, the cable undergoes measurable elongation during acceleration and braking [14, 15]. This deformation alters the effective hoisting length and induces time-varying tension forces, which excite additional vibrations in both the girder and the payload. More recent research, such as [16], showed that interaction between payload swing and payload bending in cranes carrying slender or flexible payloads can produce highly coupled and complex oscillatory patterns. These findings highlight the necessity of including both cable elasticity and girder flexibility in a unified modeling framework.

However, most existing studies consider only one elastic component (either the beam or the cable), while in practice, these components interact dynamically and generate coupled elastic–inertial vibrations of the entire system [17–19]. Furthermore, many of the existing formulations are based on partial differential equations (PDEs) [20, 21] which, although accurate, are computationally demanding and inconvenient for simulation and control synthesis. Therefore, there is a strong need to develop a nonlinear dynamic model in the form of ordinary differential equations (ODEs) that can effectively capture the key elastic characteristics of both the girder and the cable, while remaining compact and suitable for numerical analysis and control design.

Despite extensive studies, several gaps persist. (i) Most existing works rely on simplified models assuming rigid beams and payloads; (ii) the dynamic coupling between the flexible main girder, hoisting cable, and slender payload remains insuf-

ficiently investigated; (iii) the simultaneous motion of bridge, trolley, and hoisting mechanisms during acceleration–constant–deceleration phases introduces nonlinear behaviors that have not been fully characterized. Addressing these issues is crucial for improving the dynamic performance, control precision, and operational safety of modern crane systems.

The present research aims to contribute to this field by developing a comprehensive nonlinear dynamic model of an overhead crane that incorporates an elastic bridge girder, a flexible hoisting cable, and a slender suspended payload. The proposed model captures the coupled swing–bending–beam interaction under realistic operating conditions. In addition to establishing the governing equations, the study performs a detailed dynamic response analysis to evaluate the influence of system parameters and motion regimes on vibration characteristics.

2. Dynamic model of the flexible overhead crane

Consider a crane system, one typical configuration of which is illustrated in Fig. 1. The system involves three independent motions that operate in coordination during working conditions: (i) the motion of the bridge along the runway, (ii) the motion of the trolley traveling on the bridge girder, and (iii) the hoisting or lowering motion of the payload.

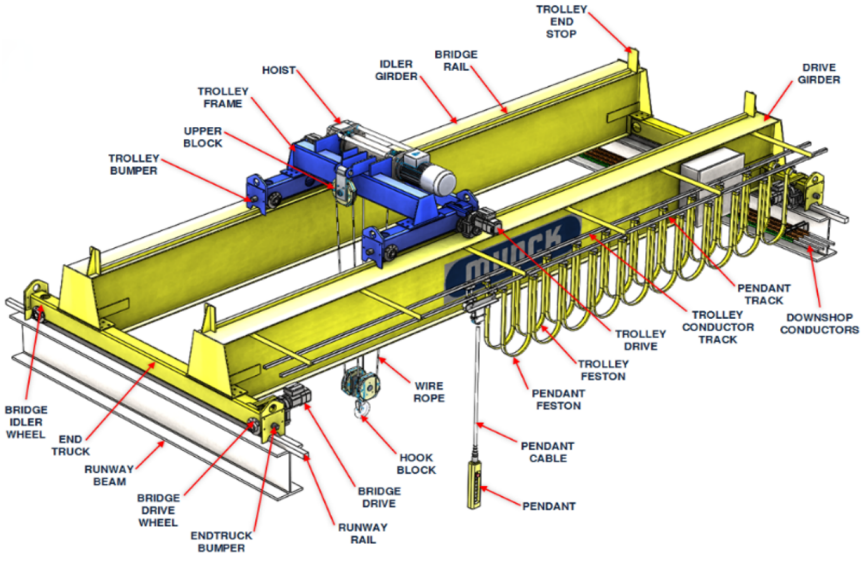

Fig. 1. Schematic diagram of an overhead crane (Munck Cranes)

In this study, the crane operation is examined in a planar working mode, where the combined motion of the trolley and the hoisting mechanism occurs in the same vertical plane. To develop the dynamic model of the crane system, the structural

decomposition method is employed. Accordingly, the system is divided into two main components:

1. The main girder, which behaves as an elastic beam subjected to moving loads; and
2. The hoisting mechanism, including the trolley and the lifting cable system, which governs the motion of the suspended payload.

2.1. Dynamic model of main girder

In previous studies most authors employed the Euler–Bernoulli beam theory, which assumes that cross-sections remain plane after deformation and neglects the effects of shear deformation and rotary inertia. This theory provides accurate results for slender beams, typically when the geometric ratio $L/h > 20$. However, for relatively thick beams, the influence of shear deformation and rotary inertia become significant, making the Euler–Bernoulli assumption less valid. In such cases, the Timoshenko beam theory, which accounts for both effects, yields more accurate results [12, 23]. For the main girder of overhead cranes, particularly for single-girder configurations with box or I-shaped cross-sections, the beam height is relatively large compared to its span length, classifying it as a moderately slender beam. Consequently, the effects of shear deformation and rotary inertia cannot be ignored. Therefore, in this study, the Timoshenko beam theory is adopted to model and analyze the vibration behavior of the main girder, ensuring a more accurate representation of the crane system's dynamic characteristics.

The beam is considered elastic according to the Timoshenko beam theory, characterized by the transverse deflection $w(x,t)$ and the rotation angle $\psi(x,t)$. The trolley, having a distance d between its two axles, exerts moving loads on the beam through the contact forces N_1 and N_2, as shown in Fig. 2.

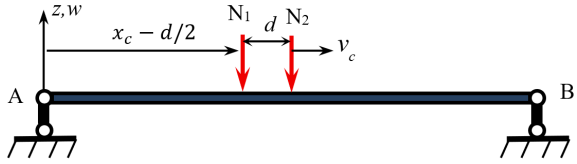

Fig. 2. Schematic of the main beam

The generalized coordinates of the beam, $w(x,t)$ and $\psi(x,t)$, respectively represent the transverse displacement and the rotation of the cross-section at position x and time t. The partial differential equations governing the transverse vibration of the beam [23] are expressed as:

$$\begin{aligned} -\frac{\partial}{\partial x}\left[kGA\frac{\partial}{\partial x}\left(\frac{\partial w}{\partial x}-\psi\right)\right]+\rho A\frac{\partial^2 w}{\partial t^2} &= f(x,t), \\ -\frac{\partial}{\partial x}\left[EI\frac{\partial \psi}{\partial x}\right]-kGA\left(\frac{\partial w}{\partial x}-\psi\right)+\rho I\frac{\partial^2 \psi}{\partial t^2} &= 0, \end{aligned} \tag{1}$$

where E, A, I, k and G denote, respectively, the Young's modulus, cross-sectional area, moment of inertia, shear correction factor, and shear modulus of the beam.

In the case of a coupled system, the governing equations take the form proposed by [24, 25], which fully account for both shear deformation and rotary inertia effects.

$$\begin{aligned} -\frac{\partial}{\partial x}\left[kGA\frac{\partial}{\partial x}\left(\frac{\partial w}{\partial x}-\psi\right)\right]+\rho A\frac{\partial^2 w}{\partial t^2}+\eta_b^t\rho A\frac{\partial w}{\partial t}=f(x,t),\\ -\frac{\partial}{\partial x}\left[EI\frac{\partial \psi}{\partial x}\right]-kGA\left(\frac{\partial w}{\partial x}-\psi\right)+\rho I\frac{\partial^2\psi}{\partial t^2}+\eta_b^s\rho I\frac{\partial\psi}{\partial t}=0 \end{aligned} \tag{2}$$

here, η_b^t and η_b^s are the shear and rotational damping coefficients of the beam, respectively, according to the Kelvin–Voigt viscoelastic model.

Using the Ritz–Galerkin expansion in terms of the beam's eigenfunctions, the approximate solutions for the beam deflection and rotation are expressed as

$$w(x,t)=\sum_{r=1}^{n_b}W_r(x)q_r(t),\quad \psi(x,t)=\sum_{r=1}^{n_b}\Psi_r(x)q_r(t). \tag{3}$$

For a beam with simply supported ends, the eigenfunctions can be written as [12, 26]:

$$W_r(x)=\sin\frac{r\pi x}{L};\quad \Psi_r(x)=g_r\cos\frac{r\pi x}{L};\quad g_r=\frac{r\pi}{L}-\frac{\omega_r^2 L\rho}{r\pi kG}, \tag{4}$$

where r is the mode number. The corresponding natural frequency ω_r of the r-th vibration mode can be determined from [23]:

$$\begin{aligned} \omega_r^4\frac{\rho\beta^2}{kG}-\omega_r^2\left(1+\frac{r^2\pi^2\beta^2}{L^2}+\frac{r^2\pi^2\beta^2}{L^2}\frac{E}{kG}\right)+\frac{\alpha^2 r^4\pi^4}{L^4}=0,\\ \alpha^2=\frac{EI}{\rho A},\quad \beta^2=\frac{I}{A}. \end{aligned} \tag{5}$$

Using the orthogonality of the particular forms, the partial differential equations (2) are reduced to ordinary differential equations of the form [12]:

$$\ddot{q}_r(t)+\eta_b\dot{q}_r(t)+\omega_r^2 q_r(t)=\frac{\int_0^L f(x,t)W_r(x)\,\mathrm{d}x}{\rho A\int_0^L W_r^2(x)\,\mathrm{d}x+\rho I\int_0^L \Psi_r^2(x)\,\mathrm{d}x}, \tag{6}$$

where

$$\int_0^L f(x,t)W_r(x)\,\mathrm{d}x = \int_0^L \left[-N_1\delta\left(x - x_c + \frac{d}{2}\right) - N_2\delta\left(x - x_c - \frac{d}{2}\right)\right]\sin\frac{r\pi x}{L}\,\mathrm{d}x$$
$$= -N_1\sin\frac{r\pi}{L}\left(x_c - \frac{d}{2}\right) - N_2\sin\frac{r\pi}{L}\left(x_c + \frac{d}{2}\right), \tag{7}$$

where $\delta(\cdot)$ denotes the Dirac delta function.

Substitute Eq. (7) into Eq. (6) to get equation

$$\ddot{q}_r(t) + \eta_b\dot{q}_r(t) + \omega_r^2 q_r(t) = -\frac{1}{m_b}\left(N_1\sin\frac{r\pi}{L}\left(x_c - \frac{d}{2}\right) + N_2\sin\frac{r\pi}{L}\left(x_c + \frac{d}{2}\right)\right), \tag{8}$$

where $m_b = \rho A\int_0^L W_r^2(x)\,\mathrm{d}x + \rho I\int_0^L \Psi_r^2(x)\,\mathrm{d}x$. Note that for Euler-Bernoulli beams the term $\Psi_r(x) = 0$. The coefficient m_b has the unit of kilogram (kg).

In case the swing angle is small, the hoist structure is symmetrical, then we can take $N_1 = N_2$.

Thus, equation (8) is the ordinary differential equation of the variable q_r ($r = 1, \ldots, n_b$). To solve this equation, we need to determine the natural frequencies of the beam.

2.2. Dynamic model of hoisting mechanism

In this case, the cable weight is assumed negligible compared to the payload weight; hence, the cable is modeled as an elastic element. Its undeformed length is denoted by $s(t)$ and its elongation by $u(t)$. The equivalent model includes an elastic spring with stiffness c and a damper with coefficient b, both depending on the cable length, as shown in Fig. 3:

$$c = n_p E_c F_c/s, \quad b = \eta_c c, \tag{9}$$

where n_p, E_c, F_c and η_c are the number of cables, the cable's elastic modulus, the cross-sectional area, and the damping coefficient according to the Kelvin–Voigt model, respectively.

The combination of cable elasticity and swinging motion generates time-varying forces acting on the main girder, which significantly affect its dynamic response.

It should be noted that in some applications, such as deep-shaft mining or offshore lifting systems, the cable length may reach several kilometers. In such cases, the cable weight and elasticity become significant, and the cable must be treated as a continuous system.

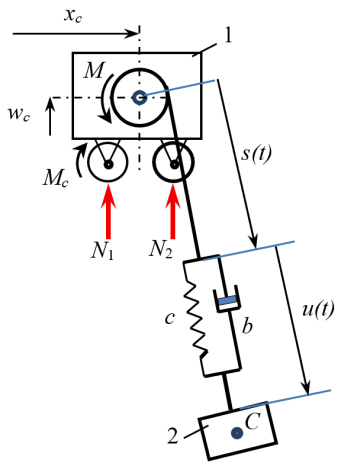

Fig. 3. Schematic of the hoisting mechanism

During hoisting, the motor torque M acts on the hoisting drum O, while the trolley motion is driven by torque M_C. The drum radius R is small compared with the cable length. The payload has a mass of m_2.

Because the cable is short and its mass is negligible, and no air resistance or other lateral disturbances are considered, the present study focuses on the longitudinal vibration of the cable while neglecting its transverse vibration.

The generalized coordinates of the trolley-hoisting system are defined as $x_c(t)$, $w_c = w(x_c, t)$, $s(t)$, $\theta(t)$, and $u(t)$, representing the trolley position, beam deflection, undeformed cable length, swing angle, and cable elongation, respectively.

Coordinates of the trolley and payload:

$$\begin{aligned} x_c &= x_c(t), & y_c &= w\left(x_c, t\right) = w_c\,, \\ x_p &= x_c + l\sin\theta, & y_p &= w_c - l\cos\theta, \end{aligned}$$

where the total cable length is $l(t) = s(t) + u(t)$.

Kinetic energy of the system:

$$\begin{aligned} T = {} & \frac{1}{2}m_1\left(\dot{x}_c^2 + \left(w_{c,t} + \dot{x}_c w_{c,x}\right)^2\right) + \frac{1}{2}J\left(\frac{\dot{s}}{R}\right)^2 \\ & + \frac{1}{2}m_2\left[\left(\dot{x}_c + \dot{l}\sin\theta + l\dot{\theta}\cos\theta\right)^2 + \left(w_{c,t} + \dot{x}_c w_{c,x} - \dot{l}\cos\theta + l\dot{\theta}\sin\theta\right)^2\right], \end{aligned} \tag{10}$$

where: m_1, m_2, J denote the mass of the trolley–hoist mechanism, the payload mass, and the rotational inertia of the drum, respectively,

$$w_{c,t} = \partial w_c/\partial t; \quad w_{c,x} = \partial w_c/\partial x.$$

Potential energy of the system:

$$\begin{aligned}\Pi &= m_1 g w_c + m_2 g\left[w_c - l\cos\theta\right] + \frac{1}{2}cu^2 \\ &= m_1 g w_c + m_2 g\left[w_c - l\cos\theta\right] + \frac{1}{2}\frac{n_p EF}{s}u^2.\end{aligned} \tag{11}$$

Dissipation function:

$$R_c = \frac{1}{2}b\dot{u}^2 = \frac{1}{2}\eta_c c\dot{u}^2 = \frac{1}{2}\frac{\eta_c n_p E_c F_c}{s}\dot{u}^2. \tag{12}$$

Generalized forces:

$$Q_{x_c} = M_c/r, \quad Q_s = -M/R, \quad Q_\theta = 0, \quad Q_u = 0, \quad Q_{w_c} = N_1 + N_2\,. \tag{13}$$

To set up the system of differential equations of motion, we use Lagrange equation in the form:

$$\frac{d}{dt}\left(\frac{\partial T}{\partial \dot{q}_j}\right) - \frac{\partial T}{\partial q_j} = -\frac{\partial \Pi}{\partial q_j} - \frac{\partial R_c}{\partial \dot{q}_j} + Q_{q_j}\,, \tag{14}$$

where $\mathbf{q} = \begin{bmatrix} x_c & s & \theta & u & w_c \end{bmatrix}^{\mathrm{T}}$ is generalized coordinate vector.

Substitute the above expressions into Eq. (14) to get the system of equations:

$$\begin{aligned}&(m_1+m_2)\left\{\begin{array}{c}\ddot{x}_c + \left[w_{c,tt} + \dot{x}_c w_{c,tx} + \ddot{x}_c w_{c,x} + \dot{x}_c\left(\dot{x}_c w_{c,xx} + w_{c,xt}\right)\right] w_{c,x} \\ + \left(w_{c,t} + \dot{x}_c w_{c,x}\right)\left(w_{c,xt} + \dot{x}_c w_{c,xx}\right)\end{array}\right\} \\ &+ m_2\begin{bmatrix}\ddot{l}\sin\theta + \dot{l}\dot{\theta}\cos\theta + \dot{l}\dot{\theta}\cos\theta + l\ddot{\theta}\cos\theta - l\dot{\theta}^2\sin\theta \\ -\ddot{l}w_{c,x}\cos\theta - \dot{l}\left(w_{c,xt} + \dot{x}_c w_{c,xx}\right)\cos\theta + \dot{l}w_{c,x}\dot{\theta}\sin\theta \\ + \left(w_{c,xt} + \dot{x}_c w_{c,xx}\right) l\dot{\theta}\sin\theta + w_{c,x}\dot{l}\dot{\theta}\sin\theta \\ + w_{c,x}l\ddot{\theta}\sin\theta + w_{c,x}l\dot{\theta}^2\cos\theta\end{bmatrix} = \frac{M_c}{r}\,,\end{aligned} \tag{15}$$

$$\begin{aligned}&m_2\ddot{x}_c\left[\sin\theta - w_{c,x}(1-\cos\theta)\right] + \ddot{s}\left[J/R^2 + m_2\sin^2\theta + m_2(1-\cos\theta)^2\right] \\ &+ \ddot{\theta}\left[m_2 l\cos\theta\sin\theta + m_2 l\sin\theta(1-\cos\theta)\right] + \ddot{u}\left[m_2\sin^2\theta + m_2(1-\cos\theta)^2\right] \\ &+ w_{c,tt}\left[-m_2(1-\cos\theta)\right] \\ &+ m_2\left(-\dot{x}_c w_{c,xt} + 2\dot{l}\dot{\theta}\sin\theta + l\dot{\theta}^2\cos\theta + \dot{x}_c w_{c,xt}\cos\theta - l\dot{\theta}^2\right) \\ &- m_2 g(1-\cos\theta) - \frac{1}{2}\frac{n_p EF}{s^2}u^2 = \frac{-M}{R}\,,\end{aligned} \tag{16}$$

$$\begin{aligned}&\ddot{x}_c l\left(\cos\theta + w_{c,x}\sin\theta\right) + \ddot{l}(0) + l^2\ddot{\theta} + w_{c,tt}l\sin\theta \\ &\quad + 2l\dot{l}\dot{\theta} + \dot{x}_c w_{c,tx}l\sin\theta + w_{c,xt}\dot{x}_c l\sin\theta + \dot{x}_c w_{c,xx}\dot{x}_c l\sin\theta = gl\sin\theta,\end{aligned} \tag{17}$$

$$m_2\ddot{x}_c\left(\sin\theta - w_{c,x}\cos\theta\right) + m_2\ddot{l} - m_2 w_{c,tt}\cos\theta + m_2\left(-2\dot{x}_c w_{c,tx}\cos\theta - \dot{x}_c\dot{x}_c w_{c,xx}\cos\theta - l\dot{\theta}^2\right) = m_2 g\cos\theta - \frac{n_p E_c F_c}{s}u - \frac{\eta_c n_p E_c F_c}{s}\dot{u}, \tag{18}$$

$$\ddot{x}_c\left(w_{c,x}m_1 + w_{c,x}m_2\right)W_c - m_2\ddot{l}W_c\cos\theta + m_2 l\ddot{\theta}W_c\sin\theta + w_{c,tt}(m_1+m_2)W_c + 2\left(m_1+m_2\right)w_{c,tx}\dot{x}_c W_c + \left(m_1+m_2\right)w_{c,xx}\dot{x}_c^2 W_c + 2m_2\dot{l}\dot{\theta}W_c\sin\theta + m_2 l\dot{\theta}^2 W_c\cos\theta + \left(m_1+m_2\right)gW_c = N_1 + N_2\,, \tag{19}$$

where

$$w_c = w(x_c,t) = \sum_{r=1}^{n_b}\sin\frac{r\pi x_c}{L}q_r\,, \quad w_{c,t} = \frac{\partial w}{\partial t}(x_c,t) = \sum_{r=1}^{n_b}\sin\frac{r\pi x_c}{L}\dot{q}_r\,,$$

$$w_{c,x} = \frac{\partial w}{\partial x}(x_c,t) = \sum_{r=1}^{n_b}\frac{r\pi}{L}\cos\frac{r\pi x_c}{L}q_r\,, \quad w_{c,tt} = \frac{\partial^2 w}{\partial t^2}(x_c,t) = \sum_{r=1}^{n_b}\sin\frac{r\pi x_c}{L}\ddot{q}_r\,,$$

$$w_{c,xx} = \frac{\partial^2 w}{\partial x^2}(x_c,t) = -\sum_{r=1}^{n_b}\left(\frac{r\pi}{L}\right)^2\sin\frac{r\pi x_c}{L}q_r\,,$$

$$w_{c,tx} = w_{c,xt} = \frac{\partial^2 w}{\partial x\partial t}(x_c,t) = \sum_{r=1}^{n_b}\frac{r\pi}{L}\cos\frac{r\pi x_c}{L}\dot{q}_r\,,$$

$$W_c = \sum_{r=1}^{n_b}W_r(x_c) = \sum_{r=1}^{n_b}\sin\frac{r\pi x_c}{L}\,.$$

The system of Eqs. (15)–(19), together with Eq. (8), is a system of nonlinear differential equations describing the dynamic response of the elastic crane system. This formulation enables a more convenient investigation of both the dynamic responses and the motion control problems of the crane compared with previously developed models, which often relied on nonlinear differential-partial differential equations with complex boundary conditions.

In this model, the main motions are driven by the control torques M and M_c. The oscillations resulting from inertial coupling (payload sway) and elastic coupling (flexural deformation of the main girder and cable elongation) must be effectively controlled or suppressed. It can thus be regarded as an underactuated vibration system, where extensive research has focused primarily on payload sway suppression, while the elastic vibrations of both the cable and the beam have received far less attention. To date, no comprehensive study has addressed the simultaneous control of inertial and elastic vibrations in such coupled crane systems, which remains an open and important direction for future research.

3. Dynamic response analysis

In this section, the dynamic responses of the crane system are analyzed through several simulation cases, including comparisons with previous studies, as well as evaluations with and without damping effects. Both the trolley motion and the hoisting drum motion are assumed to follow the same constant-acceleration profile, as shown in Fig. 4. Each motion consists of three consecutive stages: the acceleration phase (T_{on}), the constant velocity phase (T_s), and the deceleration phase (T_{off}).

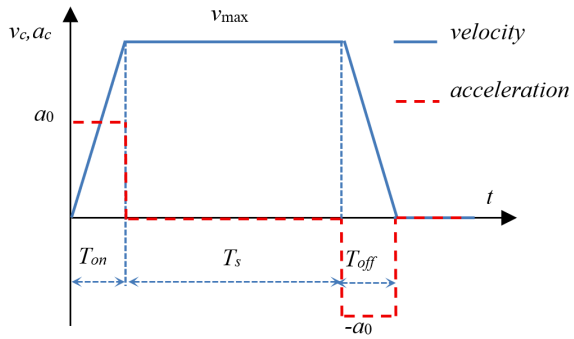

Fig. 4. Motion profile of the trolley and drum

3.1. Comparative survey

To validate the proposed dynamic model, a comparative study is carried out with the results of [9], in which the cables were considered rigid (i.e., the $u = 0$) and the cable length was constant ($s = l$ = constant). The trolley motion followed the same velocity profile as illustrated in Fig. 4. Thus, the remaining motions that need to be investigated are the swing angle of payload and elastic deformation of the main beam. The main beam model used in [9] is the Euler-Bernoulli beam model. In this study, the beam model used is the Timoshenko model. The Timoshenko model can be converted to the Euler-Bernoulli beam model with the same form as equation (8), in which the changes are [12]:

1. The natural frequencies are calculated according to the EB beam theory, determined by the formula [23]:

$$\omega_r = r^2\pi^2\sqrt{EI/\rho AL^4}, \quad r = 1, 2, \ldots \tag{20}$$

2. Equivalent modal mass m_b (neglecting rotary inertia and shear deformation)

$$m_b = \rho A \int_0^L W_r^2(x)\,\mathrm{d}x. \tag{21}$$

The beam parameters used in the simulation are taken from [9]: $E = 2.06 \times 10^{11}$ N/m^2, $L = 31$ m, $I = 0.1668$ m^4; $A = 0.1477$ m^2, $m_2 = 150\,000$ kg, $m_1 = 46\,000$ kg, $l = 6$ m, $\rho = 7820$ kg/m^3. The first natural frequency of the beam is calculated as $\omega_1 = 56.016$ rad/s and $m_b = 1.7903 \times 10^4$.

The simulation employs the same trolley motion parameters as in [9], with $v_{\max} = 0.25$ m/s, 0.33 m/s and 0.42 m/s. The trolley travels from $x_c = 0$ to $c_c = L$.

Initial conditions:

- Initial swing angle and angular velocity: $\theta(0) = 0$, $\dot{\theta}(0) = 0$;
- Initial beam deformation at the trolley position A (displacement and velocity): $w_c(0) = 0$, $\dot{w}_c(0) = 0$.

From Eqs. (3) and (4), the corresponding modal initial conditions are obtained as:

$$q_1(0) = 0 \text{ m}, \quad \dot{q}_1(0) = 0.$$

The computed mid-span deflection obtained in this study (Fig. 5a) agrees well with the reference result reported in [9] (Fig. 5b), both in terms of deformation shape and maximum amplitude. The maximum deflection at the instant when the trolley passes the mid-span is approximately 0.0342 m in this study compared with 0.0346 m in [9], corresponding to a relative error of about 1.2%. This small discrepancy demonstrates that the developed model is reliable and accurately captures the beam response. The calculations also indicate that, under the chosen motion profile, the deflection remains nearly free from noticeable residual oscillations when the trolley travels along the girder.

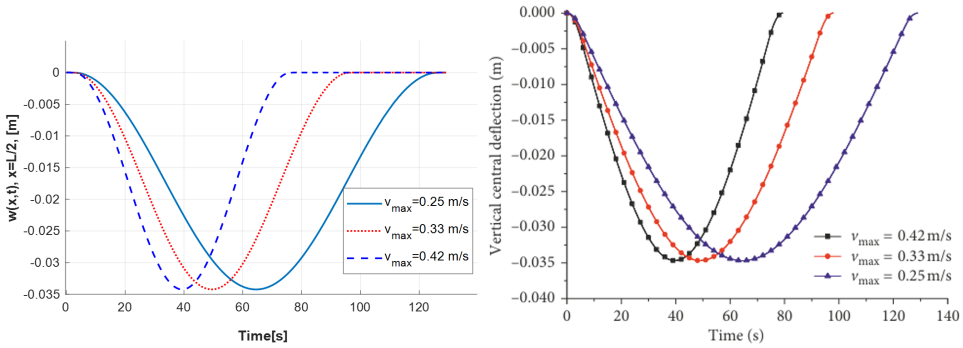

(a) This study (b) Reference [9]

Fig. 5. Vertical central deflection (m)

3.2. Dynamic response analysis without damping

In this section, the dynamic response of the developed crane model is investigated under undamped conditions. The motion profiles applied in the simulations are defined as follows:

1. *Trolley motion*: The trolley moves from the initial position $x_c = a$ to the final position $x_c = b$, according to the constant acceleration law shown in Fig. 4, with $v_{\max} = 0.25$ m/s, $T_{\text{on}} = T_{\text{off}} = 5$ s, $a = 5$ m, $b = 25$ m.
2. *Hoisting motion*: The cable length varies from $s_1 = s_{10}$ to $s_2 = s_{20}$, according to the same acceleration law as in Fig. 4 with $v_{\max} = 0.08$ m/s (4.8 m/min), $T_{\text{on}} = T_{\text{off}} = 5$ s, $s_{10} = 6$ m, $s_{20} = 16$ m. The variation of trolley position and cable length is illustrated in Fig. 6. In this analysis, both the trolley and the hoisting motions are activated simultaneously (excluding cable elasticity).

Beam parameters: The beam parameters are chosen according to the reference [9]. The additional parameters of the Timoshenko beam for calculation are $G = 0.81 \times 10^{11}$ N/m^2 (steel), $k = 5/6$ (rectangular cross section), $d = 1.1$ m. The natural frequency of the beam determined by solving equation (5) is $\omega_1 = 54.755$ rad/s ($\omega_2 = 206.057$, $\omega_3 = 426.206$, ...). Previous applications of the Ritz–Galerkin method have shown that the fundamental mode typically captures the dominant portion of the deformation energy, while the contribution of higher modes decreases rapidly. Consequently, the literature generally recommends retaining only the first mode ($n_b = 1$) when very high accuracy is not required, or the first three modes ($n_b = 3$) when a more refined approximation is desired, while the use of more than five modes is seldom reported. For this reason, and to reduce computational complexity while maintaining acceptable accuracy, the present study adopts the fundamental-mode truncation, i.e., $n_b = 1$.

Cable parameters: The hoisting cable has a diameter $D = 36$ mm, number of cables $n_p = 16$, $E_c = 1.41 \times 10^{11}$ N/m^2, $F_c = f\pi D^2/4$, $f = 0.59$ is fill factor.

Initial conditions:

- Initial swing angle and angular velocity: $\theta(0) = 0$, $\dot{\theta}(0) = 0$;
- Initial beam deformation (Timoshenko beam):

$$w_c(a,0) = -N\left(\frac{a^2(L-a)^2}{3EIL} + \frac{a(L-a)}{kGAL}\right), \qquad \dot{w}_c(a,0) = 0.$$

Here, N denotes the total weight of the trolley–payload system, $N = (m_1 + m_2)g$. With the system parameters, the static deflection is computed as:

$$w_c(a,0) = w_c(5,0) = -0.00703 \text{ m}.$$

From Eqs. (3) and (4), the corresponding modal initial conditions are obtained as:

$$q_1(0) = -0.01451 \text{ m}, \quad \dot{q}_1(0) = 0.$$

The dynamic responses of the overhead crane under these conditions are shown in Figs. 7–11, payload swing angle (Fig. 7), cable elongation (Fig. 8), mid-span beam deflection (Fig. 9). Fig. 10 illustrates the beam deflection corresponding to the instantaneous position of the moving trolley (x_c), and Fig. 11 shows the deflection of the entire beam at the instant when the trolley passes the mid-span position ($t = T_0$).

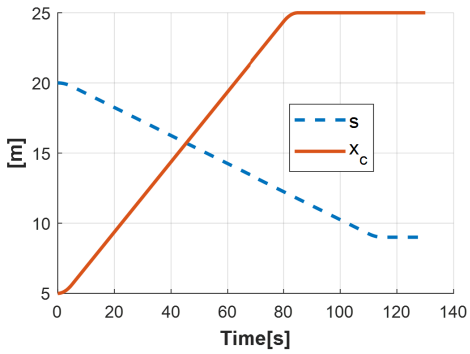

Fig. 6. The trolley (x_c) and the hoisting motions (s)

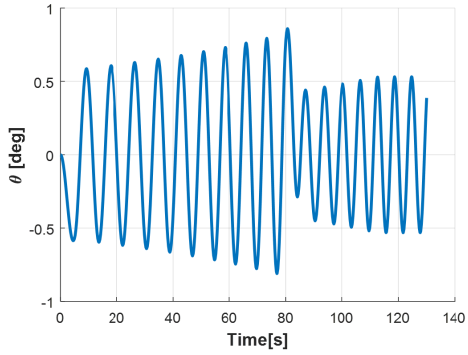

Fig. 7. Payload swing angle

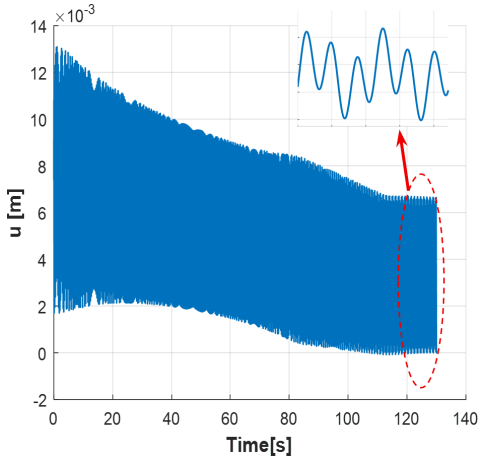

Fig. 8. Cable elongation

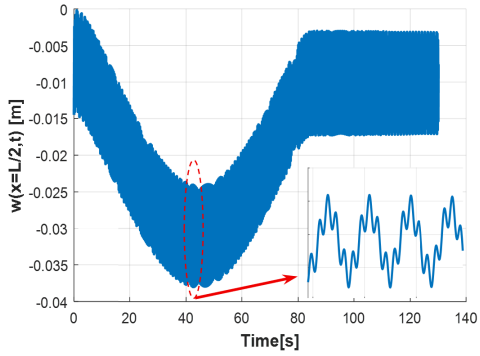

Fig. 9. Mid-span beam deflection

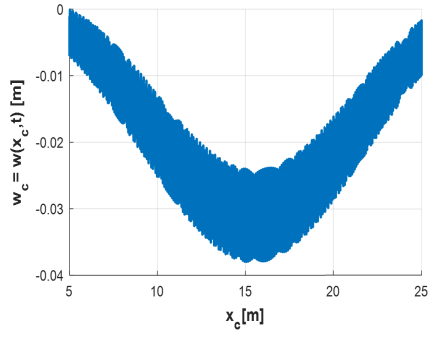

Fig. 10. Deflection corresponding to x_c

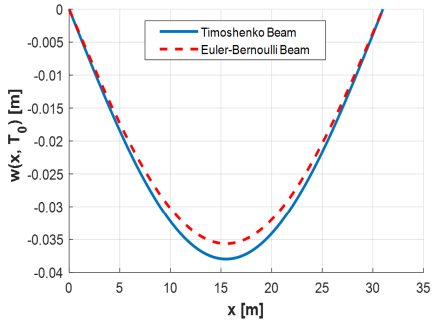

Fig. 11. Deflection of the beam at T_0

From the results we see that:

- The payload exhibits periodic swing oscillations throughout the trolley and hoisting motion. The maximum swing angle is approximately $\pm 1^\circ$, which is within a realistic range for industrial cranes operating at moderate speeds. This confirms that the excitation induced by the trolley acceleration is the dominant source of sway.
- The elastic deformation of the cable reaches its maximum when the cable is the longest ($s = 20$ m), with an amplitude of about 13 mm. This deformation gradually decreases as the cable shortens to its minimum length ($s = 6$ m) where it is approximately 6.5 mm. The elastic deformation exhibits periodic oscillations that do not decay because structural damping is not included in the model. These elastic oscillations act as an additional source of excitation contributing to the deformation of the main girder.
- The maximum deflection at the beam mid-span, $w_{\max}(x = L/2) = 0.0380$ m, shows only a small deviation from the previous study, which did not account for cable deformation ($w_{\max}(x = L/2) = 0.0346$ m [9]). However, a noticeable difference is observed in the elastic oscillation amplitude, which reaches approximately 0.014 m at the mid-span. Even after the motion has ceased, the free elastic oscillation remains relatively large, with an amplitude of about 0.011 m. The vibration response contains both low- and high-frequency components, corresponding to the sway motion and the elastic coupling of the beam and cable, respectively. In contrast, previous studies reported that elastic oscillations had negligible amplitudes, low frequencies, and decayed rapidly once the motion stopped.
- Figure 11 shows that when the Euler–Bernoulli beam theory is used, the maximum deflection is $w_{\max}(x = L/2) = 0.0356$ m; whereas using the Timoshenko beam theory gives $w_{\max}(x = L/2) = 0.0380$ m, a deviation of about 6.7%. This indicates that the error is significant when applying the Euler-Bernoulli model compared with the more accurate Timoshenko formulation. It is expected that this discrepancy would be even larger for single-girder bridge cranes, where the beam depth is relatively large compared to its span length.

3.3. Dynamic response analysis with damping

Case study 1: In this case, the parameters are the same as those used in the previous analysis (Section 3.2). The damping coefficients are selected as $\eta_c = 2 \times 10^{-4}$ s^{-1} for the cable and $\eta_b = 1 \times 10^{-3}$ s^{-1} for the beam. The computed dynamic responses are shown in Fig. 12 (cable elongation) and Fig. 13 (mid-span beam deflection).

From Figs. 12–13, it can be observed that introducing the damping coefficients markedly alters the vibration characteristics of both the crane beam and the hoisting cable. The maximum beam deflection decreases from 0.0380 m to 0.0338 m, while

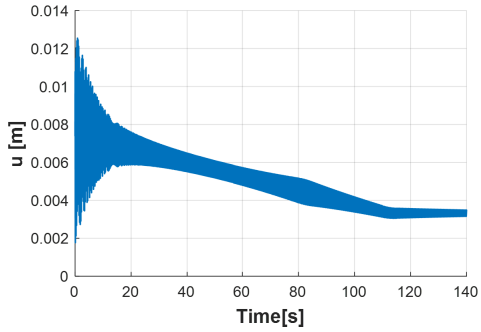

Fig. 12. Cable elongation

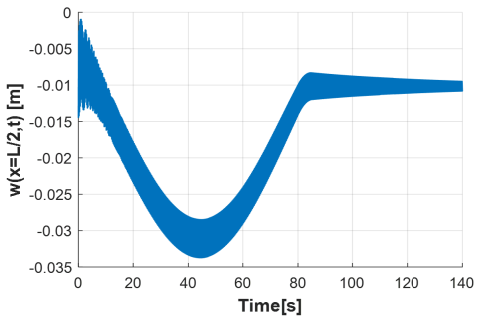

Fig. 13. Mid-span beam deflection

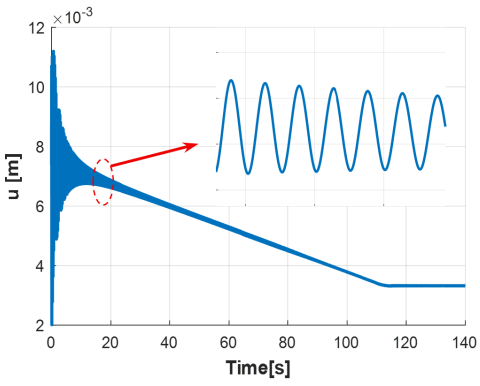

Fig. 14. Cable elongation

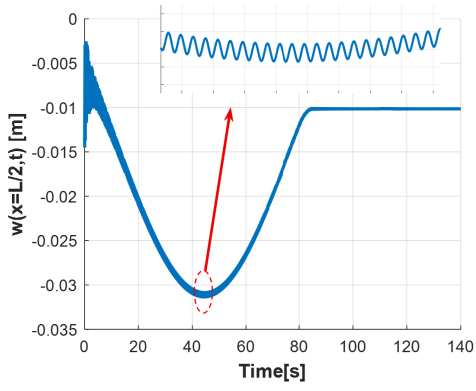

Fig. 15. Mid-span beam deflection

the maximum cable elongation reduces from 0.014 m to 0.0125 m. Moreover, the amplitudes of elastic oscillation in both the cable and the beam are significantly attenuated. The free vibrations gradually decay over time, which is consistent with the typical behavior of a damped oscillatory system.

Case study 2: In this case, the cable damping coefficient is increased to $\eta_c = 2 \times 10^{-3}$ s^{-1}, while the beam damping is set to $\eta_b = 0$. The purpose of this study is to investigate the influence of the cable damping coefficient on the attenuation of elastic oscillations in both the beam and the cable. Figs. 14–15 present the mid-span beam deflection and the cable elongation, respectively. It can be observed that the deflection of the beam and the elongation of the cable are almost completely damped, and the elastic oscillations converge toward their static deformation states. However, the time required for the oscillations to reach static equilibrium remains relatively long.

In another analysis, when the cable damping was set to $\eta_c = 0$ and the beam damping increased to $\eta_b = 5 \times 10^{-3}$ s^{-1} the dynamic response was found to be similar to the undamped case ($\eta_c = 0, \eta_b = 0$). This behavior can be explained by the fact that the forced elastic oscillations are mainly induced by the sway motion

and the elastic deformation of the cable. As long as the excitation source persists, the oscillations are maintained, and the damping effect on the beam alone has limited influence.

Through the above survey, we can see that increasing the cable resistance not only reduces the amplitude of the cable's stretching oscillation but also reduces the deflection amplitude of the beam, proving that the elastic oscillation of the cable is the main source of excitation causing the beam to oscillate. Therefore, controlling or optimizing the cable's resistance coefficient can be considered an effective solution to control the elastic oscillation of the entire crane system. Adding or controlling the shock absorber properly for the cable will help to significantly reduce the elastic oscillation, improve the stability, accuracy in operation and structural life of the elastic crane system.

4. Conclusion

This study developed a planar dynamic model of an elastic overhead crane, in which both the flexural deformation of the main girder and the axial elongation of the hoisting cable were taken into account. In addition, internal damping effects caused by material friction were incorporated into the formulation. The resulting equations of motion form a nonlinear system of ordinary differential equations (ODEs), which provides a compact and convenient representation for analyzing the dynamic responses, vibration control, and stability of the crane system. Compared with previous studies that typically yielded partial differential equation (PDE) models, the present approach offers a simpler yet sufficiently accurate framework that still captures the essential elastic–inertial coupling phenomena of the system.

The numerical investigations lead to the following main findings:

i) The primary source of elastic vibration in the main girder originates from the axial deformation of the hoisting cable, while the payload sway motion (caused by trolley acceleration) also contributes to the vibration coupling;

ii) When cable elasticity is considered, the maximum beam deflection increases only slightly compared with the inextensible-cable case, but the amplitude of elastic oscillation becomes significantly larger. In the absence of damping, these oscillations persist even after the main motion stops;

iii) The damped simulations reveal that the damping coefficients can be effectively tuned to suppress elastic vibrations of both the beam and the cable. In combination with previously developed payload sway control strategies, the proposed model provides a foundation for designing integrated vibration control schemes that enhance the stability, accuracy, and operational performance of flexible overhead cranes.

References

[1] V.S. Loveikin and Y.O. Romasevych. Antisway control of suspended loads under variable operating conditions. *Archive of Mechanical Engineering*, 70(3):367–385, 2023. doi: 10.24425/ame.2023.146842.

[2] E. Molina-Santana, M.R. Ferrer-Cepero, F. Gonzalez-Montañez, J.U. Liceaga-Castro, V.M. Jimenez-Mondragon, and J.C. Olivares-Galvan. Generalized framework for designing a linear control scheme for regulating a sub-actuated overhead crane. *International Journal of Dynamics and Control*, 13:168, 2025. doi: 10.1007/s40435-025-01669-8.

[3] M.R. Mojallizadeh, B. Brogliato, and C. Prieur. Modeling and control of overhead cranes: a tutorial overview and perspectives. *Annual Reviews in Control*, 56:1–42, 2023. doi: 10.1016/j.arcontrol.2023.03.002.

[4] T.K. Nguyen. Combination of feedback control and spring-damper to reduce the vibration of crane payload. *Archive of Mechanical Engineering*, 68(2):165–173, 2021. doi: 10.24425/ame.2021.137046.

[5] T.G. Duong. Determining parameters to optimize the pulling force for the luffing jib tower cranes by Taguchi method. *Archive of Mechanical Engineering*, 70(3):387–407, 2023. doi: 10.24425/ame.2023.146845.

[6] A. Al-Fadhli and K. Alghanim. Dynamic modeling and optimization of lifting mechanisms under nonlinear constraints. *Archive of Mechanical Engineering*, 72(2):199–219, 2025.

[7] S. Chwastek and S. Michalowski. Suppression of crane vibrations with controlled boom support system. *Archive of Mechanical Engineering*, 48(1):19–28, 2001.

[8] A. Maczyński. Determination of drive functions of slewing of a mobile crane which minimize load oscillations. *Archive of Mechanical Engineering*, 50(2):167–180, 2003.

[9] H. Liu, W. Cheng, and Y. Li. Dynamic responses of an overhead crane's beam subjected to a moving trolley with a pendulum payload. *Shock and Vibration*, Article ID 1291652, 14 pages, 2019. doi: 10.1155/2019/1291652.

[10] V.H. Trinh. Study of dynamic response of crane system via surrogates based on Karhunen–Loève expansion and neural networks. *Journal of Science and Technology in Civil Engineering (HUCE)*, 17(2):193–202, 2023. doi: 10.31814/stce.huce2023-17(2)-17.

[11] G.D. Muscă and S. Năstac. Dynamic modelling of overhead crane. *IOP Conference Series: Materials Science and Engineering*, 916(1):012071, 2020. doi: 10.1088/1757-899X/916/1/012071.

[12] N.T.V. Huong, N.S. Nam, and N.V. Khang. Numerical evaluation of the forced vibration response of a Timoshenko beam subjected to a moving force using the modal analysis approach. *Journal of Science and Technology: Engineering and Technology for Sustainable Development*, 32(1):61–70, 2022. doi: 10.51316/jst.156.etsd.2022.32.1.9.

[13] C. Yang, J. Huang, and W. Singhose. Dynamic coupling analysis of flexible slender payloads in overhead cranes. *Mechanical Systems and Signal Processing*, 220:111676, 2024. doi: 10.1016/j.ymssp.2024.111676.

[14] K.S. Hong and U.H. Shah. *Dynamics and Control of Industrial Cranes*. Springer Nature Singapore, 2019. doi: 10.1007/978-981-13-5770-1.

[15] A. Arena, A. Casalotti, W. Lacarbonara, and M.P. Cartmell. Dynamics of container cranes: three-dimensional modeling, full-scale experiments, and identification. *International Journal of Mechanical Sciences*, 93:8–21, 2015. doi: 10.1016/j.ijmecsci.2014.11.024.

[16] N.Đ. Zrnić, V.M. Gašić, S.M. Bošnjak, and M. Đorđević. Moving loads in structural dynamics of cranes: bridging the gap between theoretical and practical researches. In *Proceedings of the 11th International Conference on Vibration Problems (ICOVP)*, Lisbon, Portugal, 9–12 September 2013.

[17] V.H. Trinh, N.H. Thua, H.D. Tuan, and P.V. Hieu. Failure probability analysis of overhead crane bridge girders within uncertain design parameters. *Journal of Science and Technology in Civil Engineering (NUCE)*, 14(3):125–135, 2020. doi: 10.31814/stce.nuce2020-14(3)-11.

[18] K.S. Hong and U.H. Shah. Modeling, distributed parameter analysis, and control of flexible cranes. In *Advances in Industrial Control*. Springer, Singapore, 2019.

[19] V.S. Loveikin, Y.O. Romasevych, and O.V. Zhukov. Vibration control and optimization in underactuated lifting systems. *Archive of Mechanical Engineering*, 70(3):355–366, 2023.

[20] P. Arena, F. Famoso, and L. Fortuna. Nonlinear modeling and control of cranes: from theory to industrial application. *Mechanical Systems and Signal Processing*, 203:109103, 2023. doi: 10.1016/j.ymssp.2023.109103.

[21] L. Nguyen, T. Do, and N. Tran. Analytical modeling of elastic cables and damping effects in large-scale crane systems. *Archive of Mechanical Engineering*, 72(1):41–59, 2025. doi: 10.24425/ame.2025.153739.

[22] V.H. Trinh and P.V. Hieu. Probabilistic safety assessment of industrial cranes under variable loading conditions. *Archive of Mechanical Engineering*, 70(4):421–438, 2023. doi: 10.24425/ame.2023.146847.

[23] S.S. Rao, *Vibration of Continuous Systems*. John Wiley & Sons, 2007.

[24] P. Hagedorn and A. DasGupta. *Vibrations and waves in continuous mechanical systems*. John Woley & Sons, 2007.

[25] A.W. Leissa and M.S. Qatu. *Vibration of Continuous Systems*. McGraw-Hill, 2011.

[26] T. Kim, I. Park, and U. Lee. Forced vibration of Timoshenko beam subjected to stationary and moving loads using the modal analysis method. *Shock and Vibration*, 2017; 1–26, doi: 10.1155/2017/3924921.